IEEE Access
Multidisciplinary | Rapid Review | Open Access Journal

Received 7 December 2023, accepted 20 December 2023, date of publication 25 December 2023, date of current version 3 January 2024.

Digital Object Identifier 10.1109/ACCESS.2023.3347193

RESEARCH ARTICLE

Efficient Frequency and Time-Domain Simulations of Delayed PEEC Models With Proper Orthogonal Decomposition Techniques

MUHAMMAD A. KHATTAK[1,2], DANIELE ROMANO[1], GIULIO ANTONINI[1], (Senior Member, IEEE), AND FRANCESCO FERRANTI[3], (Senior Member, IEEE)

[1]Department of Industrial and Information Engineering and Economics, University of L'Aquila, 67100 L'Aquila, Italy
[2]Department of Applied Physics and Photonics, Brussels Photonics, Vrije Universiteit Brussel, 1050 Brussels, Belgium
[3]Department of Applied Physics and Photonics, Brussels Photonics, Vrije Universiteit Brussel and Flanders Make, 1050 Brussels, Belgium

Corresponding author: Muhammad A. Khattak (muhammadaltaf.khattak@graduate.univaq.it)

The work of Francesco Ferranti was supported in part by the Methusalem and Hercules Foundations, and in part by the Research Council (OZR) of Vrije Universiteit Brussel (VUB).

ABSTRACT The Partial Element Equivalent Circuit (PEEC) method has gained significant recognition as an electromagnetic computational technique known for its ability to represent electromagnetic phenomena using equivalent circuits. This feature makes it particularly valuable for addressing mixed EM-circuit problems. However, PEEC models often exhibit large dimensions, necessitating modeling techniques that can effectively reduce their size while preserving accuracy. Model order reduction (MOR) serves as a highly effective approach to accomplish this objective. This paper presents two MOR techniques based on proper orthogonal decomposition (POD) for PEEC models described by neutral delayed differential equations (NDDEs). The unique characteristics of NDDEs demand specialized MOR approaches, as their formulation is inherently more complex compared to standard quasi-static PEEC models described by non-delayed differential equations. In addition to a traditional one-shot singular value decomposition (SVD), this paper also presents an incrementally computed SVD to evaluate the orthogonal matrix needed to generate the reduced order matrices. The accuracy and efficiency of the proposed PEEC-MOR methods are demonstrated through multiple relevant numerical results in both the frequency-domain and time-domain.

INDEX TERMS Partial element equivalent circuit (PEEC) method, model order reduction, proper orthogonal decomposition, frequency-domain analysis, time-domain analysis.

I. INTRODUCTION

Computational electromagnetic (EM) methods [1], [2], [3] are used to analyze the electromagnetic behavior of complex EM systems. The Partial Element Equivalent Circuit (PEEC) method is an EM method commonly used in electromagnetic compatibility (EMC) analysis, interconnect, and antenna design. In such a method, the dielectric and conductive areas of the system are discretized, and a set of elements known as partial elements are used to represent the mesh cells. The partial elements are linked together to build an equivalent circuit that represents the whole EM system behavior.

The PEEC models that are quasi-static can be represented using a series of Ordinary Differential Equations (ODEs) [4]. Nonetheless, for complex electrically long structures where propagation delays play a significant role, the delayed PEEC models have proven to be more suitable for accurately describing their EM behavior. These delayed PEEC models

The associate editor coordinating the review of this manuscript and approving it for publication was Ladislau Matekovits.

are formulated using a series of Neutral Delayed Differential Equations (NDDEs) [4].

PEEC models often exhibit large dimensions, e.g., a large number of state variables and corresponding state-space matrices, which leads to the need for modeling techniques that can effectively reduce their size while preserving accuracy. Model order reduction (MOR) techniques [5] offer a means to decrease the complexity of dynamical models while maintaining an accurate representation of their input-output behavior, specifically their transfer function. In EM analysis, MOR can be employed with PEEC models to significantly reduce their computational cost, enabling more efficient resolution of complex EM problems while still achieving precise results for the analyzed systems. Although MOR techniques for systems described by (non-delayed) differential equations [5], [6], [7], [8], [9] are well-established, the focus on MOR techniques for delayed differential equations and delayed PEEC models is a relatively recent research area [10], [11], [12], [13], [14]. In [11], a moment-matching MOR technique was developed specifically for delayed PEEC models. This method involves calculating the system's moments using additional state variables while expanding the exponential factors $e^{-s\tau_k}$ via a Taylor series. In [12], a multiorder Arnoldi algorithm was introduced to reduce delayed PEEC models using moment-matching MOR. Notably, the multiorder Arnoldi algorithm in [12] allows for the implicit calculation of the moments of the original system without the need for introducing extra state variables. Both [11] and [12] ensure that the reduced PEEC models remain in the form of NDDEs and therefore retain the structure of the original delayed PEEC models.

In this paper, we present two MOR techniques for delayed PEEC models where a one-shot and an incremental SVD approach are used in a proper orthogonal decomposition (POD) framework. POD has been commonly used in various problems from fluid dynamics [15] to inverse problems [16]. POD is a general technique to identify a low-dimensional representation of the key system behavior, which proves useful in a variety of ways. The most common use is to project the original system equations onto a reduced-order subspace defined by the POD basis vectors, which generates a POD-based reduced-order model. Time-domain or frequency-domain simulations of the original system can be the source of information needed to extract the POD basis vectors [17], [18], [19], [20], [21], [22]. No moment matching is required. The only information needed is to sample the behavior of the original system (this sampled information is called snapshots). The incremental SVD instead of a one-shot SVD allows flexibility at multiple levels, from avoiding the need to have all snapshots together as in a one-shot SVD to being able to incrementally add snapshots if needed [23], [24], [25]. These POD-based MOR approaches for delayed PEEC models preserve the neutral delayed differential structure in the reduced order models. These MOR methods can also have applications in other domains where large-scale delayed differential equations are present. Frequency-domain and time-domain simulations can be performed by the generated reduced-order models. A two-step time-domain integration method was used to obtain time-domain results and it is described in this paper. A brief outline limited to a one-shot SVD POD technique for frequency-domain simulations of delayed PEEC models was introduced in [26]. The main novel contributions of this paper with respect to [26] are

- the development of the incremental SVD-based POD MOR algorithm for delayed PEEC models;
- the development of a time-domain solver for delayed PEEC models and an extensive comparison among multiple models (original and reduced order models based on multiple MOR techniques) in the time-domain in addition to the frequency-domain;
- the implementation of two numerical examples with a higher number of delays in the delayed PEEC models with respect to the only example in [26].

Multiple pertinent numerical results validate the MOR techniques proposed in this paper for both frequency-domain and time-domain analyses. A detailed comparison among original PEEC models, POD MOR techniques based on a one-shot and an incremental SVD, and a multipoint moment matching MOR technique is provided.

II. PROBLEM BACKGROUND AND PROPOSED MOR APPROACH

The PEEC method utilizes integral equations (IE) to analyze electromagnetic (EM) phenomena by representing them in the form of a circuit. The PEEC variant we present here relies on the widely recognized Volume Equivalence Principle [27], enabling the creation of highly precise models for the crucial EM phenomena found in contemporary electric and electronic devices.

The fundamental building blocks of a PEEC model consist of partial inductances, denoted as $L_{p_{mn}}$, and potential coefficients, represented as $P_{\ell,m}$.

In the context of a system consisting of two volumes, denoted as V_n and V_m, through which electric current densities are assumed to flow, the magnetic interaction between them is captured by the mutual partial inductance. This mutual partial inductance can be expressed in the Laplace domain as [4]:

$$L_{p_{m,n}}(s) = \frac{\mu_0}{4\pi}\frac{1}{S_m S_n}\int_{V_m}\int_{V_n} \hat{\boldsymbol{u}}_m \cdot \hat{\boldsymbol{u}}_n \frac{e^{-s\tau}}{|\boldsymbol{r}_m - \boldsymbol{r}_n|} dV_n dV_m \quad (1)$$

where S_n and S_m represent the sections traversed by the corresponding currents. The local unit vectors normal to these sections are denoted as $\hat{\boldsymbol{u}}_n$ and $\hat{\boldsymbol{u}}_m$ respectively. Additionally, $\boldsymbol{r}_n$ and $\boldsymbol{r}_m$ refer to the position vectors that identify internal points within the two volumes. The term $\tau = \frac{|\boldsymbol{r}_m - \boldsymbol{r}_n|}{c_0}$ is the free-space time delay between the points $\boldsymbol{r}_n, \boldsymbol{r}_m$.

Likewise, when contemplating a system comprising two surfaces labeled as S_ℓ and S_m, where superficial electric charge densities are present, the coefficient of potential governing their electric interaction can be articulated within

the Laplace domain as follows:

$$P_{\ell,m}(s) = \frac{1}{4\pi\varepsilon_0}\frac{1}{S_\ell S_m}\int_{S_\ell}\int_{S_m}\frac{e^{-s\tau}}{|\boldsymbol{r}_\ell - \boldsymbol{r}_m|}dS_m dS_\ell \quad (2)$$

The integrals in equations (1) and (2) employ the free space Green's function, which incorporates the time delay between each pair of distant points. This capability is facilitated by the Volume Equivalence Principle, as outlined in [27].

The computation of equations (1) and (2) can be significantly simplified by making certain approximations. An accurate approximation, known as center to center (CC), involves approximating the time delay τ with the time required by the electromagnetic field to traverse the distance between the spatial supports of two basis functions [4]. This approximation is better suited for simulating electrically large structures. With the center-to-center approximation, the partial inductance can be expressed as:

$$L_{p_{m,n}}(s) = \frac{\mu_0}{4\pi}\frac{e^{-s\tau_L}}{S_m S_n}\int_{V_m}\int_{V_n}\hat{\boldsymbol{u}}_m\cdot\hat{\boldsymbol{u}}_n\frac{1}{|\boldsymbol{r}_m - \boldsymbol{r}_n|}dV_n dV_m \quad (3)$$

and the coefficient of potential:

$$P_{\ell,m}(s) = \frac{1}{4\pi\varepsilon_0}\frac{e^{-s\tau_P}}{S_\ell S_m}\int_{S_\ell}\int_{S_m}\frac{1}{|\boldsymbol{r}_\ell - \boldsymbol{r}_m|}dS_\ell dS_m \quad (4)$$

where τ_L is computed as the propagation delays between the centers of the supporting domains V_m and V_n and τ_P between the centers of S_ℓ and S_m.

III. FULL-WAVE PEEC MODELS

By employing the center-to-center approximation to compute the partial elements, the MNA form of PEEC models can be derived in a matrix form and it reads

$$\mathbf{C}(t)\frac{d\mathbf{x}(t)}{dt} = -\mathbf{G}(t)\mathbf{x}(t) + \mathbf{B}\mathbf{u}(t) \quad (5a)$$

$$\mathbf{y}(t) = \mathbf{L}^T\mathbf{x}(t) \quad (5b)$$

where the vector of the unknowns $\mathbf{x}(t) \in \Re^{n_u\times 1}$ is given as

$$\mathbf{x}(t) = \begin{bmatrix}\mathbf{i}(t) & \boldsymbol{\phi}_{sr}(t) & \boldsymbol{\phi}_i(t) & \mathbf{v}_d(t) & \mathbf{q}_s(t)\end{bmatrix}^T, \quad (6)$$

where $\mathbf{i}(t)$ are the branch currents, $\boldsymbol{\phi}_{sr}(t)$ are the scalar potentials for surface nodes, $\boldsymbol{\phi}_i(t)$ are the scalar potentials for internal nodes, $\mathbf{v}_d(t)$ are the excess capacitance voltages for dielectric branches, and $\mathbf{q}_s(t)$ represent the surface charges. Furthermore, the state space matrices $\mathbf{C}(t)$, $\mathbf{G}(t)$ and $\mathbf{B}$ are:

$$\mathbf{C}(t) = \begin{bmatrix} \underset{n_b\times n_b}{\mathbf{L}_p(t)*} & \underset{n_b\times n_{ns}}{\mathbf{0}} & \underset{n_b\times n_{ni}}{\mathbf{0}} & \underset{n_b\times n_{bd}}{\mathbf{0}} & \underset{n_b\times n_p}{\mathbf{0}} \\ \underset{n_{ns}\times n_b}{\mathbf{0}} & \underset{n_{ns}\times n_{ns}}{\mathbf{0}} & \underset{n_{ns}\times n_{ni}}{\mathbf{0}} & \underset{n_{ns}\times n_{bd}}{\mathbf{0}} & \underset{n_{ns}\times n_p}{\mathbf{M}^T} \\ \underset{n_{ni}\times n_b}{\mathbf{0}} & \underset{n_{ni}\times n_{ns}}{\mathbf{0}} & \underset{n_{ni}\times n_{ni}}{\mathbf{0}} & \underset{n_{ni}\times n_{bd}}{\mathbf{0}} & \underset{n_{ni}\times n_p}{\mathbf{0}} \\ \underset{n_{bd}\times n_b}{\mathbf{0}} & \underset{n_{bd}\times n_{ns}}{\mathbf{0}} & \underset{n_{bd}\times n_{ni}}{\mathbf{0}} & \underset{n_{bd}\times n_{bd}}{\mathbf{C}_d} & \underset{n_{bd}\times n_p}{\mathbf{0}} \\ \underset{n_p\times n_b}{\mathbf{0}} & \underset{n_p\times n_{ns}}{\mathbf{0}} & \underset{n_p\times n_{ni}}{\mathbf{0}} & \underset{n_p\times n_{bd}}{\mathbf{0}} & \underset{n_p\times n_p}{\mathbf{0}} \end{bmatrix}, \quad (7)$$

$$\mathbf{G}(t) = \begin{bmatrix} \underset{n_b\times n_b}{\mathbf{R}} & \underset{n_b\times n_{ns}}{\mathbf{A}_s} & \underset{n_b\times n_{ni}}{\mathbf{A}_i} & \underset{n_b\times n_{bd}}{\Gamma} & \underset{n_b\times n_p}{\mathbf{0}} \\ \underset{n_{ns}\times n_b}{-\mathbf{A}_s^T} & \underset{n_{ns}\times n_{ns}}{\mathbf{0}} & \underset{n_{ns}\times n_{ni}}{\mathbf{0}} & \underset{n_{ns}\times n_{bd}}{\mathbf{0}} & \underset{n_{ns}\times n_p}{\mathbf{0}} \\ \underset{n_{ni}\times n_b}{-\mathbf{A}_i^T} & \underset{n_{ni}\times n_{ns}}{\mathbf{0}} & \underset{n_{ni}\times n_{ni}}{\mathbf{0}} & \underset{n_{ni}\times n_{bd}}{\mathbf{0}} & \underset{n_{ni}\times n_p}{\mathbf{0}} \\ \underset{n_{bd}\times n_b}{-\Gamma^T} & \underset{n_{bd}\times n_{ns}}{\mathbf{0}} & \underset{n_{bd}\times n_{ni}}{\mathbf{0}} & \underset{n_{bd}\times n_{bd}}{\mathbf{0}} & \underset{n_{bd}\times n_p}{\mathbf{0}} \\ \underset{n_p\times n_b}{\mathbf{0}} & \underset{n_p\times n_{ns}}{-\mathbf{M}} & \underset{n_p\times n_{ni}}{\mathbf{0}} & \underset{n_p\times n_{bd}}{\mathbf{0}} & \underset{n_p\times n_p}{\mathbf{P}(t)*} \end{bmatrix}, \quad (8)$$

$$\mathbf{B} = \begin{bmatrix} \underset{n_b\times n_b}{\mathcal{I}} & \underset{n_b\times n_{ns}}{\mathbf{0}} \\ \underset{n_{ns}\times n_b}{\mathbf{0}} & \underset{n_{ns}\times n_{ns}}{\mathcal{I}} \\ \underset{n_{ni}\times n_b}{\mathbf{0}} & \underset{n_{ni}\times n_{ns}}{\mathbf{0}} \\ \underset{n_{bd}\times n_b}{\mathbf{0}} & \underset{n_{bd}\times n_{ns}}{\mathbf{0}} \\ \underset{n_p\times n_b}{\mathbf{0}} & \underset{n_p\times n_{ns}}{\mathbf{0}} \end{bmatrix}, \quad (9)$$

where $*$ represents the convolution operator, and n_b, n_{ns}, n_{ni}, n_{bd} and n_p represent the cardinality of branches, surface nodes, internal nodes, dielectric cells and surface cells, respectively. Moreover, $\mathbf{C}_d$ is the excess capacitance matrix [28], $\mathbf{R}$ is the branches resistance matrix, $\mathbf{A}_s$ is the incidence matrix for the surface nodes, $\mathbf{A}_i$ is the incidence matrix for the internal nodes, Γ is the dielectric region selection matrix, and $\mathbf{M}$ is the surface-to-node reduction matrix.

The time-dependent partial inductance matrix $\mathbf{L}_p(t)$ and the coefficient of potential matrix $\mathbf{P}(t)$ are derived from (3) and (4) and read

$$\mathbf{L}_p(t) = \mathbf{L}_{p,0}\delta(t) + \sum_{k=1}^{n_{\tau_L}}\mathbf{L}_{p,k}\delta(t-\tau_{L,k}), \quad (10a)$$

$$\mathbf{P}(t) = \mathbf{P}_0\delta(t) + \sum_{q=1}^{n_{\tau_P}}\mathbf{P}_k\delta(t-\tau_{P,q}), \quad (10b)$$

where the matrices $\mathbf{L}_{p,0}$ and $\mathbf{P}_0$ account for the delayless magnetic and electric couplings while $\mathbf{L}_{p,k}, k = 1,\cdots,n_{\tau_L}$, and $\mathbf{P}_k, k = 1,\cdots,n_{\tau_P}$ take the propagation delay into account;n_{τ_L} is the number of significant delays between elementary volumes while n_{τ_P} is the number of significant delays between elementary surfaces; $\tau_{L,i} = R_{cc,i}/c_0, i = 1,\cdots,n_{\tau_L}$ and $\tau_{P,q} = R_{cc,q}/c_0, q = 1,\cdots,n_{\tau_P}$ denote the delays between the centers, identified by $R_{cc,i}$ and $R_{cc,q}$ respectively, of the spatial supports of the basis functions of currents and charges; c_0 is the speed of the light in the background medium. Finally, the source vector $\mathbf{u}(t)$ is given as

$$\mathbf{u} = \begin{bmatrix}\mathbf{v}_s(t)\\ \mathbf{i}_s(t)\end{bmatrix}, \quad (11)$$

where $\mathbf{v}_s(t)$ and $\mathbf{i}_s(t)$ are the voltage and current sources, which are applied to branches and nodes, respectively.

Equations (5) form a system of delayed differential equations of the neutral type (NDDEs), where the delays exist not only in the state vector $\mathbf{x}(t)$ but also in its time derivative $d\mathbf{x}(t)/dt$. Each delayed component in the matrices $\mathbf{C}(\boldsymbol{\tau})$ and $\mathbf{G}(\boldsymbol{\tau})$ acts as a delay operator for the

corresponding component in the vector $\mathbf{x}(t)$. Therefore, (5) can be reformulated in the Laplace domain as:

$$s\mathbf{C}(s)\mathbf{X}(s) = -\mathbf{G}(s)\mathbf{X}(s) + \mathbf{B}\mathbf{U}(s) \tag{12a}$$
$$\mathbf{Y}(s) = \mathbf{B}^T\mathbf{X}(s) \tag{12b}$$
$$\mathbf{C}(s) = \mathbf{C}_0 + \sum_{k=1}^{n_{\tau_{Lp}}} \mathbf{C}_k e^{-s\tau_{L,k}} \tag{12c}$$
$$\mathbf{G}(s) = \mathbf{G}_0 + \sum_{k=1}^{n_{\tau_P}} \mathbf{G}_k e^{-s\tau_{P,k}}. \tag{12d}$$

IV. PROPER ORTHOGONAL DECOMPOSITION MOR TECHNIQUE

A reduced-order model can be written as

$$s\mathbf{C}_r(s)\mathbf{X}_r(s) = -\mathbf{G}_r(s)\mathbf{X}_r(s) + \mathbf{B}_r\mathbf{U}(s) \tag{13a}$$
$$\mathbf{Y}(s) = \mathbf{B}_r^T\mathbf{X}_r(s) \tag{13b}$$
$$\mathbf{C}_r(s) = \mathbf{C}_{r,0} + \sum_{k=1}^{n_{\tau_L}} \mathbf{C}_{r,k} e^{-s\tau_{L,k}} \tag{13c}$$
$$\mathbf{G}_r(s) = \mathbf{G}_{r,0} + \sum_{k=1}^{n_{\tau_P}} \mathbf{G}_{r,k} e^{-s\tau_{P,k}} \tag{13d}$$

where the following congruence transformations based on the orthogonal matrix $\mathbf{K} \in \Re^{n_u \times n_r}$ are employed

$$\mathbf{C}_{r,i} = \mathbf{K}^T\mathbf{C}_i\mathbf{K}, \quad i = 0, \ldots, n_{\tau_{L_p}} \tag{14a}$$
$$\mathbf{G}_{r,i} = \mathbf{K}^T\mathbf{G}_i\mathbf{K}, \quad i = 0, \ldots, n_{\tau_P} \tag{14b}$$
$$\mathbf{B}_r = \mathbf{K}^T\mathbf{B} \tag{14c}$$
$$\mathbf{L}_r = \mathbf{K}^T\mathbf{L} \tag{14d}$$

The same reduced order model in the time domain can be written as

$$\mathbf{C}_{r,0}(t)\frac{d\mathbf{x}_r(t)}{dt} = -\mathbf{G}_{r,0}(t)\mathbf{x}_r(t) - \sum_{k=1}^{n_{\tau_L}} \mathbf{C}_{r,k}\frac{dx_r}{dt}(t-\tau_k) - \sum_{k=1}^{n_{\tau_P}} \mathbf{G}_{r,k}x_r(t-\tau_k) + \mathbf{B}_r\mathbf{u}(t) \tag{15a}$$
$$\mathbf{y}(t) = \mathbf{L}_r^T\mathbf{x}_r(t) \tag{15b}$$

where the vector $\mathbf{x}_r(t)$ represents the reduced state variables. NDDEs (15) can be rewritten in a more compact form as:

$$\mathbf{C}_{r,0}\frac{d\mathbf{x}_r(t)}{dt} + \mathbf{G}_{r,0}\mathbf{x}_r(t) = \mathbf{T} + \mathbf{B}_r\mathbf{u}(t), \tag{16}$$

where

$$\mathbf{T} = -\sum_{k=1}^{n_{\tau_L}} \mathbf{C}_{r,k}\frac{dx_r}{dt}(t-\tau_k) - \sum_{k=1}^{n_{\tau_P}} \mathbf{G}_{r,k}x_r(t-\tau_k) \tag{17}$$

.

Concerning time-domain simulations of delayed PEEC models, assuming a uniform time step, NDDEs (15a) can be integrated using one or two-step integration methods. The general form of the solution using two-step methods reads:

$$\alpha\frac{d\mathbf{x}(t)}{dt} = \mu_p\mathbf{x}_p + \mu_{p-1}\mathbf{x}_{p-1} + \mu_{p-2}\mathbf{x}_{p-2} - \beta\frac{d\mathbf{x}_{p-1}(t)}{dt}, \tag{18}$$

where the subscript p identifies the time step and homogeneous initial conditions are set for $\mathbf{x}_{p-1}$, $\mathbf{x}_{p-2}$, and $\frac{d\mathbf{x}_{p-1}(t)}{dt}$. The coefficients for each of the methods are given in Table 1.

TABLE 1. Time integration methods.

Integration Method	$\mu_\mathbf{p}$	$\mu_{\mathbf{p-1}}$	$\mu_{\mathbf{p-2}}$	α	β
BE (Backward Euler)	1/h	−1/h	0	1	0
BD2 (Gear)	1.5/h	−2/h	1/(2h)	1	0
Trapezoidal	1/h	−1/h	0	0.5	0.5
Theta θ	1/h	−1/h	0	θ	$1-\theta$

Applying the scheme (18) to (16), we obtain

$$\frac{\mu_p}{\alpha}\mathbf{C}_{r,0}\mathbf{x}_p + \mathbf{G}_{r,0}\mathbf{x}_p = \mathbf{B}\mathbf{u}_p + \mathbf{T}_p - \mathbf{C}_{r,0}\left(\frac{\mu_{p-1}}{\alpha}\mathbf{x}_{p-1} + \frac{\mu_{p-2}}{\alpha}\mathbf{x}_{p-2} - \frac{\beta}{\alpha}\frac{d\mathbf{x}_{p-1}(t)}{dt}\right), \tag{19}$$

where $\mathbf{T}_p$ is the time discrete counterpart of $\mathbf{T}$ in (16). The same time-domain simulation approach can be used for both original and reduced order PEEC models. As it will be shown in the numerical results, time-domain simulations of the POD-based reduced order models will be much faster than the original delayed PEEC models, while a high accuracy is preserved. A two-step time-domain integration method was used to obtain time-domain results shown in the numerical examples.

The construction of the orthogonal basis $\mathbf{K}$ plays a crucial role in obtaining a compact and accurate reduced-order model across a wide frequency range. Although MOR techniques for systems described by (non-delayed) differential equations [5], [6], [7], [8], [9] are well-established, the focus on MOR techniques for delayed differential equations and delayed PEEC models is a relatively recent research area [10], [11], [12], [13], [14]. In [11] and [12], moment-matching MOR techniques were proposed for PEEC models described by NDDEs. The calculation of moments for the MOR step can lead to a significant computational cost to generate the orthogonal matrix needed for the computation of the reduced order matrices. Also, it requires the availability in memory of the full original matrices that can be very large. POD-based MOR is a solution to these issues of the moment matching MOR.

POD-based MOR is commonly used in various problems ranging from fluid dynamics [15] to inverse problems [16] and partial differential equations (PDEs) constrained optimization problems [29]. Time-domain or frequency-domain

simulations of the original system can be the source of information needed to extract the POD basis vectors [17], [18], [19], [20], [21], [22], [30]. In this work, we consider snapshots in the frequency-domain. Considering a set of q frequencies $s \in \{s_1, s_2, \ldots, s_q\}$ ($s = j\omega$), then the corresponding snapshots at this given set of frequencies are represented as

$$\mathbf{X}_{\text{ss}} = [\Re(\mathcal{H}(s_1)), \Im(\mathcal{H}(s_1)), \ldots, \Re(\mathcal{H}(s_q)), \Im(\mathcal{H}(s_q))] \quad (20)$$

where $\mathbf{X}_{\text{ss}} \in \Re^{n_u \times q}$ represents the snapshot matrix and

$$\mathcal{H}(s) = (s\mathbf{C}(s) + \mathbf{G}(s))^{-1}\mathbf{B} \quad (21)$$

Applying singular value decomposition (SVD) to the snapshot matrix

$$\mathbf{X_{ss}} = \mathbf{U}\Sigma\mathbf{V}^T, \quad (22)$$

where $\mathbf{U} = [\mathbf{u}_1, \mathbf{u}_2, \ldots, \mathbf{u}_q] \in \Re^{n \times q}$ and $\mathbf{V} = [\mathbf{v}_1, \mathbf{v}_2, \ldots, \mathbf{v}_q] \in \Re^{n \times q}$ are orthogonal matrices $\Sigma \in \Re^{q \times q}$ represents the singular values of $\mathbf{X_{ss}}$ at diagonals i.e. $diag(\sigma_1, \sigma_2, \ldots, \sigma_q)$. A truncation on the maximum number of singular values can be used to decide the reduced order n_r.

The $\mathbf{V}$ matrix is used as the orthogonal matrix $\mathbf{K}$ needed to generate the reduced order matrices by congruence transformations.

In a traditional POD approach, a one-shot traditional SVD decomposition is applied to the snapshot matrix $\mathbf{X_{ss}}$ to extract an orthogonal matrix needed for the congruence transformations. In addition to this traditional SVD decomposition, in this work, we also explore the concept of incrementally computed singular value decomposition (INCR-SVD) in which the SVD of the whole matrix is not evaluated but rather the singular vectors are constructed incrementally [23], [24], [25]. This can provide computational advantages and flexibility in adding snapshots incrementally. The main idea behind this is to use subsequent additive modifications of the snapshot matrix where new snapshots are incrementally added. The reader can refer to [23], [24], and [25] for extensive details on the implementation of the incremental SVD. We report in what follows the main notions related to the incremental SVD. It allows flexibility at multiple levels, from avoiding the need to have all snapshots together as in a one-shot SVD to being able to incrementally add snapshots if needed. To formulate the incrementally computed SVD, we have the following steps:

1) Let us consider the snapshot matrix $\mathbf{X}_{ss}$ defined in (22), then we define

$$\mathbf{A}_1 = \mathbf{X}_{ss}(:, 1 : m), \quad (23)$$
$$\mathbf{A}_2 = \mathbf{X}_{ss}(:, m + 1 : q). \quad (24)$$

where $\mathbf{A}_1 \in \mathbb{R}^{n_u \times m}$, $\mathbf{A}_2 \in \mathbb{R}^{n_u \times q-m}$ and m is the number of snapshots that formed the initial snapshot matrix of which an SVD is performed.

2) We apply a standard SVD to $\mathbf{A}_1$ as

$$\mathbf{A}_1 = \mathbf{U}_1\Sigma_1\mathbf{V}_1^T, \quad (25)$$

Next, we assume to update the initial SVD of $\mathbf{A}_1$ by considering a block of k columns of $\mathbf{A}_2$ inside a loop till all columns of $\mathbf{A}_2$ are considered as better clarified in what follows.

3) For each block of k columns of $\mathbf{A}_2$, we define

$$\mathbf{M} = \mathbf{U}_1^\top \mathbf{A}_2(:, k * (i-1) + 1 : k * i)) \quad (26)$$
$$\mathbf{P} = \mathbf{A}_2(:, k * (i-1) + 1 : k * i)) - \mathbf{U}_1\mathbf{M} \quad (27)$$

4) We evaluate the QR factorization of $\mathbf{P}$

$$[\mathbf{Q}_P\mathbf{R}_P] = qr(\mathbf{P}) \quad (28)$$

When k is small, this algorithm is invoked frequently, and algebraic subspace rotations involved possibly do not preserve orthogonality. Hence, a numerically induced loss of orthogonality of the matrix $\begin{bmatrix}\mathbf{U}_1 & \mathbf{Q}_P\end{bmatrix}$ may occur. Therefore, we apply the QR decomposition to it as shown in (29)

$$[\mathbf{Q}_Q\ \mathbf{R}_Q] = qr(\begin{bmatrix}\mathbf{U}_1 & \mathbf{Q}_P\end{bmatrix}) \quad (29)$$

5) We then evaluate the SVD decomposition $\mathbf{U}_P\,\Sigma_P, \mathbf{V}_P$ of $\mathbf{D}$ which is defined as

$$\mathbf{D} = \mathbf{R}_Q \begin{bmatrix}\Sigma_1 & \mathbf{M} \\ 0 & \mathbf{R}_P\end{bmatrix} \quad (30)$$

We evaluate the incrementally updated SVD as:

$$\widetilde{\Sigma}_P = \Sigma_P(1 : t, 1 : t) \quad (31)$$
$$\widetilde{\mathbf{V}}_P = \begin{bmatrix}\mathbf{V} & 0 \\ 0 & \mathbf{I}\end{bmatrix}\mathbf{V}_P(1 : t, 1 : t) \quad (32)$$
$$\widetilde{\mathbf{U}}_P = \mathbf{Q}_Q\mathbf{U}_P(1 : t, 1 : t) \quad (33)$$

where t can be used as a rank truncation threshold. If no truncation is performed, then t is sum of number of columns of $\mathbf{U}_1$ and $\mathbf{P}$.

6) Finally, we update

$$\Sigma_1 = \widetilde{\Sigma}_P, \mathbf{V}_1 = \widetilde{\mathbf{V}}_P, \mathbf{U}_1 = \widetilde{\mathbf{U}}_P \quad (34)$$

The steps 3-6 are repeated for the different blocks of columns of $\mathbf{A}_2$ till all columns of $\mathbf{A}_2$ are considered.

Low rank truncation and parallelization strategies can be important to enhance the computational efficiency of the incremental SVD. As an example, the QR factorization can be implemented in efficient ways by using parallelism approaches [31]. The incremental SVD can work by adding a column vector at a time or a matrix with a certain number of columns at a time to an original SVD decomposition. The steps of the incremental SVD-based POD MOR technique we propose for delayed PEEC models are described in Algorithm 1. It is to be noted that if new snapshot information needs to be added and a standard one-shot SVD approach is used, a new one-shot SVD needs to be performed of the previous snapshot matrix augmented by the new snapshot vectors.

This algorithm is used to generate the orthonormal basis $\mathbf{K} \in \Re^{n_u \times n_r}$ required to build the reduced order model in (15) through subsequent congruence transformations.

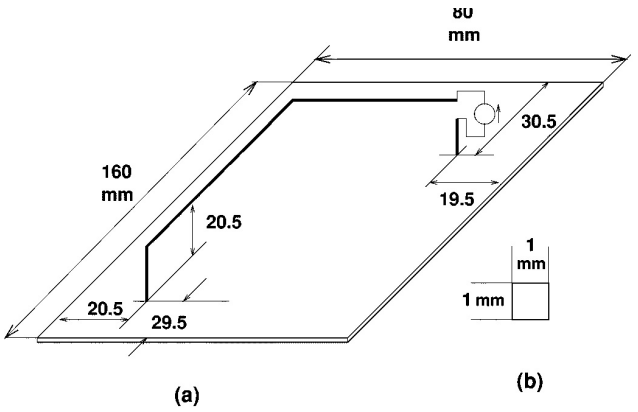

FIGURE 1. Geometry of the L-shaped conductor over a ground plane.

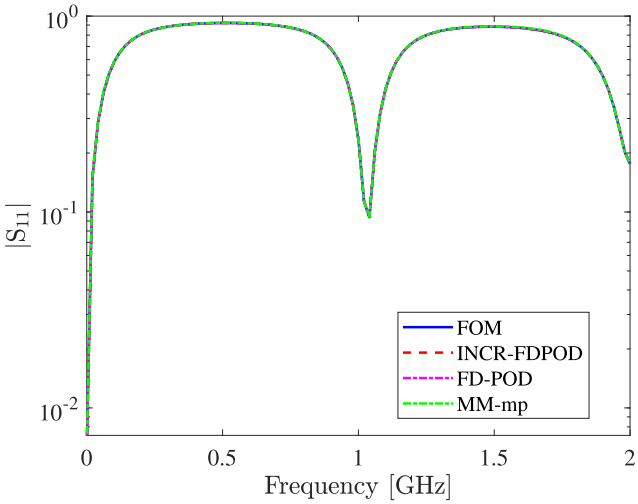

FIGURE 2. Magnitude of S_{11} for the L-shaped conductor over the ground plane example.

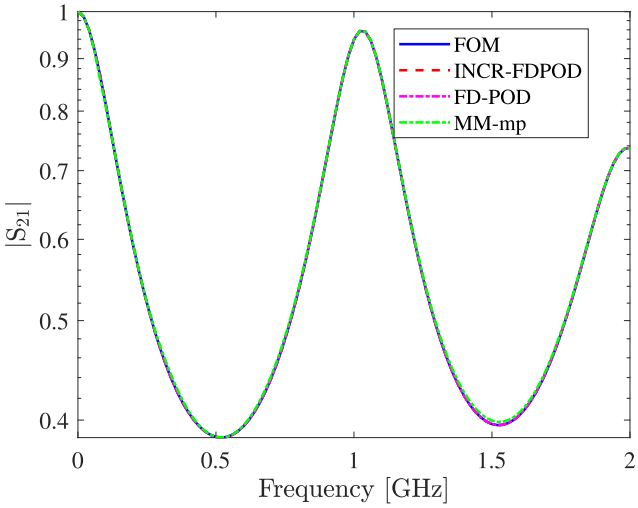

FIGURE 3. Magnitude of S_{21} for the L-shaped conductor over the ground plane example.

In the case of a one-shot SVD, the operation mentioned as INCR − SVD in Algorithm 1 is replaced by a standard SVD. The operation INCR − SVD in Algorithm 1 could also be combined with an adaptive selection of the snapshot samples,

Algorithm 1 INCR-FDPOD for Delayed PEEC Models

Inputs: $\mathbf{C}$, $\mathbf{G}$, $\mathbf{B}$ & n_p = number of ports, k = columns of $\mathbf{A}_1$, m= columns of $\mathbf{X}_{ss}$
Output: $\mathbf{K}$
Initialization: $i = 1$; $\mathbf{X} = []$; q = number of singular vectors to be chosen; n_r = order of the reduced order model
Consider $s = s_1, s_2, \ldots, s_q$ on the imaginary axis and construct snapshot matrix as $\mathcal{H}_{1,\ldots,n_p}(s)$
WHILE $i <= n_p$
Get snapshot vectors i.e. $\mathbf{X}_i = [\Re(\mathcal{H}_i(s)), \Im(\mathcal{H}_i(s))]$;
$i = i + 1$;
END WHILE
Construct $\mathbf{A}_1$ and $\mathbf{A}_2$; % Eq. (23) and Eq. (24)
Compute $\mathbf{U}_1$, Σ_1, $\mathbf{V}_1$ by a standard SVD
FOR i=1:$\lceil((q-m)/k)\rceil$
Define $\mathbf{M}$ and $\mathbf{P}$; % Eq. (26) and Eq. (27)
Find $\mathbf{Q}_P$ and $\mathbf{R}_P$; % Eq. (28)
Find $\mathbf{Q}_Q$ and $\mathbf{R}_Q$; % Eq. (29)
Evaluate the updated SVD % Eq. (31) to Eq. (33)
Update $\Sigma_1 = \widetilde{\Sigma}_P$, $\mathbf{V}_1 = \widetilde{\mathbf{V}}_P$, $\mathbf{U}_1 = \widetilde{\mathbf{U}}_P$
END FOR
Choose $\mathbf{K} = \mathbf{U}_1$.

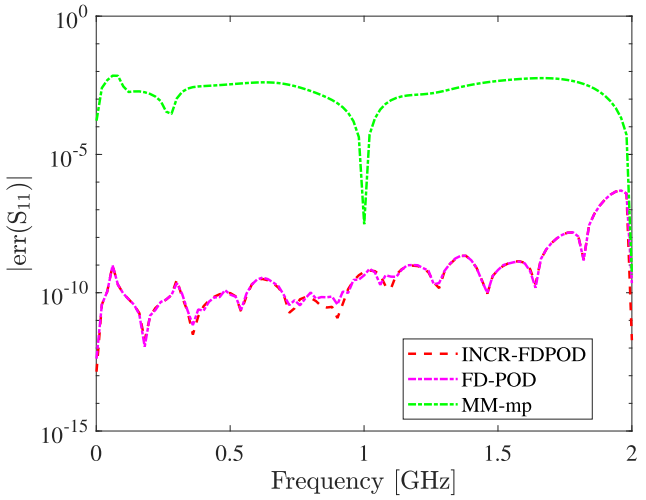

FIGURE 4. Reduced order models error comparison for S_{11} for the L-shaped conductor over the ground plane example.

but this is beyond the scope of this work and an objective for future work.

V. NUMERICAL RESULTS

To test our methodology, we consider two different examples of MOR of delayed PEEC models. We denote the full original model as FOM, while the model constructed using Algorithm 1 is denoted by INCR-FDPOD, and the standard POD with a one-shot SVD is denoted as FD-POD. FD stands for frequency-domain since we use snapshots in the frequency-domain to build the reduced order models. We also compare the results with the multipoint expansion moment matching method [12] denoted as MM-mp.

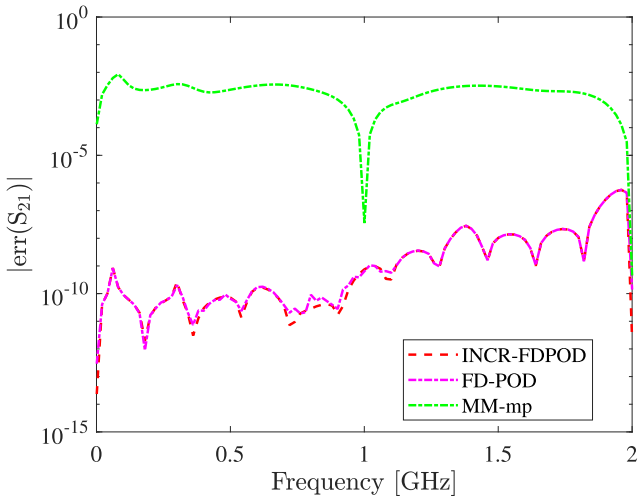

FIGURE 5. Reduced order models error comparison for S_{21} for the L-shaped conductor over the ground plane example.

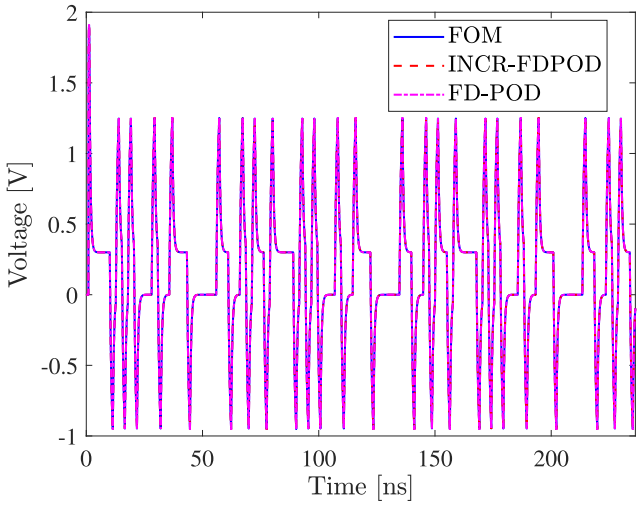

FIGURE 6. Comparison of the first port voltage for the L-shaped conductor over the ground plane example.

All the tests were performed with the MATLAB R2021a [32] on a Windows 10 pro platform having Intel(R) Xeon(R) CPU X5677 @ 3.47GHz 3.46 GHz (2 processors) and 176 GB RAM.

A. L-SHAPED CONDUCTOR OVER A GROUND PLANE

The proposed MOR approach has been tested on the L-shaped conductor over a ground plane sketched in Fig. 1. The conductors are assumed to be copper. The original model entails $n_u = 9707$ degrees of freedom with $n_I = 2$ inputs and $n_O = 2$ outputs. There are $n_{\tau_L} = 294$ and $n_{\tau_P} = 297$ delays for the magnetic and electric field couplings, respectively. Using Algorithm 1, we obtain a POD-based reduced order model of size $n_r = 48$ utilizing 12 snapshots uniformly distributed in the frequency range [1 MHz, 2 GHz]. The computation of the **K** matrix of the INCR-FDPOD and FD-POD methods has been carried out by using the INCR-SVD and one-shot standard SVD methods, respectively. In the case of $MM-mp$, we use three expansion points [10 Hz, 1 GHz, 2 GHz] and we obtain a reduced order model of the same size. A CPU time comparison related to the construction of the different reduced order models and the size of each reduced model are shown in Table 2.

We also analyze the CPU time needed to evaluate the scattering parameters for a frequency sample by the different models and we illustrate it in Table 3.

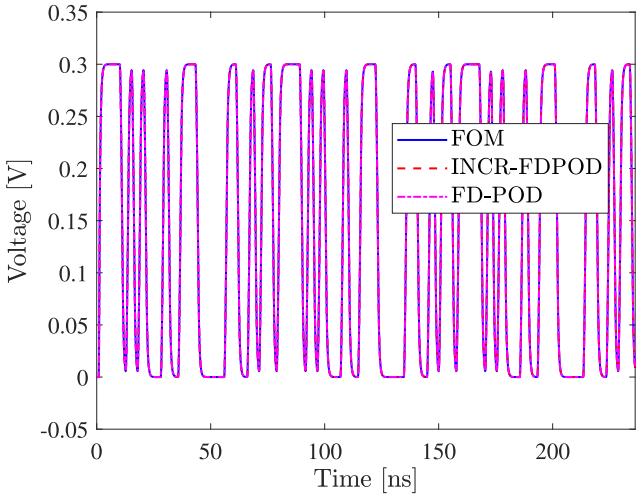

FIGURE 7. Comparison of the second port voltage for the L-shaped conductor over the ground plane example.

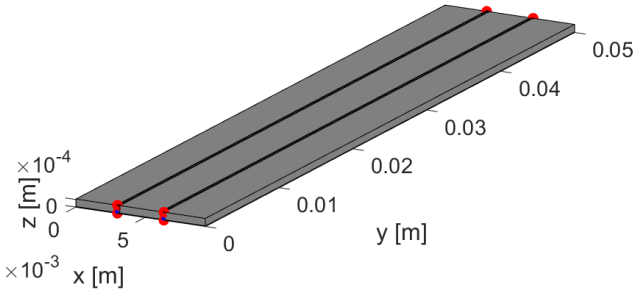

FIGURE 8. Two microstrip interconnection.

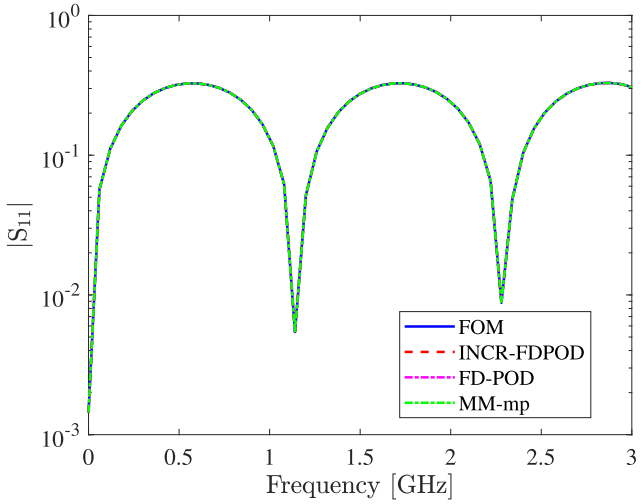

FIGURE 9. Magnitude of S_{11} for the two microstrip interconnection example.

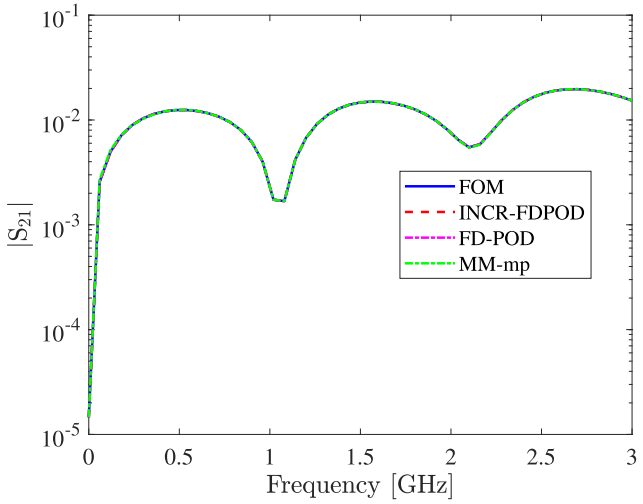

FIGURE 10. Magnitude of S_{21} for the two microstrip interconnection example.

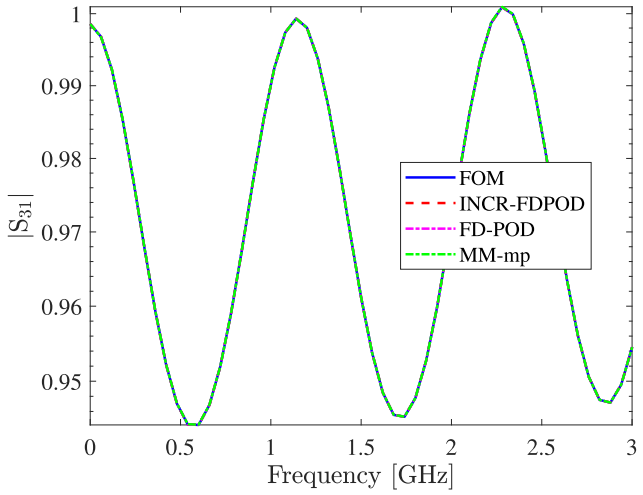

FIGURE 11. Magnitude of S_{31} for the two microstrip interconnection example.

TABLE 2. Construction time and size of the reduced order models for the L-shaped conductor over a ground plane example.

Model	Size	Construction Time (s)
FOM-dir	9707	-
INCR-FDPOD	48	3464
FD-POD	48	3403
MM-mp	48	7269

TABLE 3. CPU time comparison for a single frequency sample evaluation of the scattering parameters for the L-shaped conductor over a ground plane example.

Model	Evaluation Time (s)
FOM	344
INCR-FDPOD	$1.185 \cdot 10^{-2}$
FD-POD	$1.161 \cdot 10^{-2}$
MM-mp	$1.543 \cdot 10^{-2}$

To assess the accuracy of the reduced order models in comparison with the FOM, we generate a plot illustrating the magnitude spectra of the scattering parameters. Figs. 2-3 show the magnitude spectra of the S_{11} and S_{21} parameters, respectively as obtained by the FOM and the reduced order models.

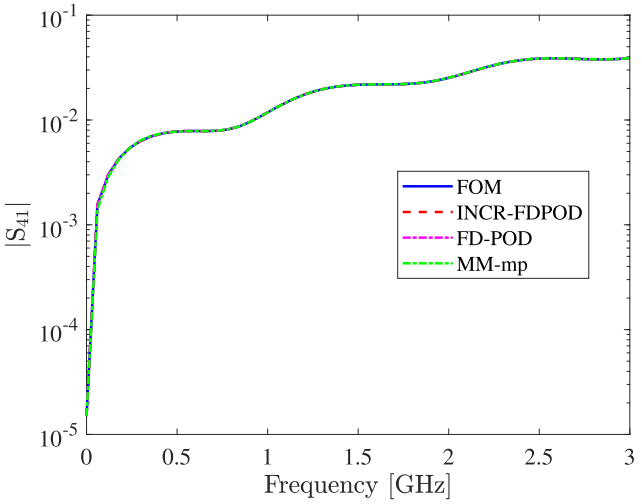

FIGURE 12. Magnitude of S_{41} for the two microstrip interconnection example.

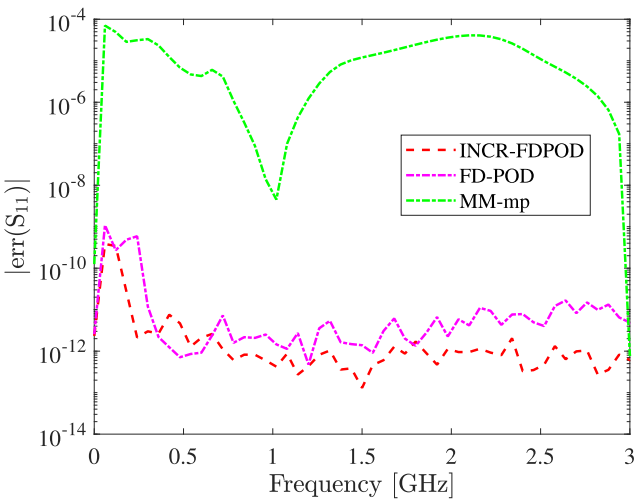

FIGURE 13. Reduced order models error comparison for S_{11} for the two microstrip interconnection example.

To assess the accuracy of both reduced order models, we compare the error of S_{11} and S_{21} for all the ROMs shown in Figs. 4-5 The errors show that INCR-FDPOD and FD-POD perform better than MM-mp in terms of accuracy. Next, we analyze some time-domain results by exciting the first input with a pseudorandom binary sequence (PRBS) voltage source and comparing the port voltages. The voltage on the first port is depicted in Fig. 6. Similarly, the voltage of the second port is shown in Fig. 7.

It required 2755 s to obtain time-domain results with the FOM, whereas the INCR-FDPOD and FD-POD models achieved this in just 9 s and 8 s, respectively. Notably, the reduced-order models generated using the INCR-FDPOD and FD-POD methods consistently produce accurate and stable time-domain results, in contrast to the MM-mp generated model that exhibits instability in the time-domain.

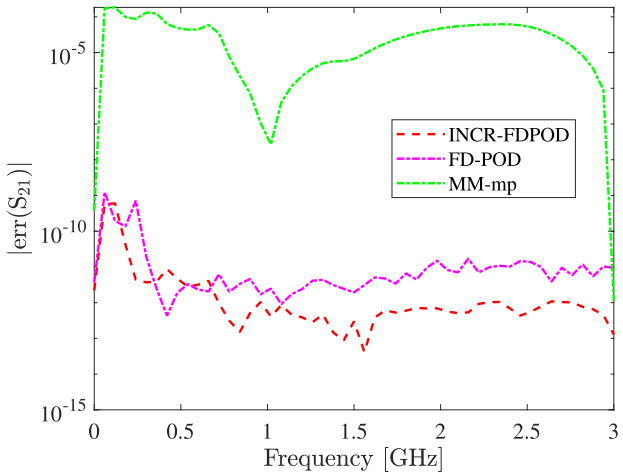

FIGURE 14. Reduced order models error comparison for S_{21} for the two microstrip interconnection example.

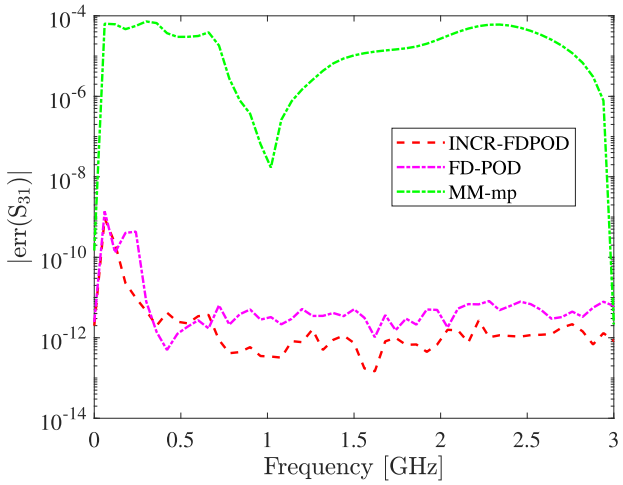

FIGURE 15. Reduced order models error comparison for S_{31} for the two microstrip interconnection example.

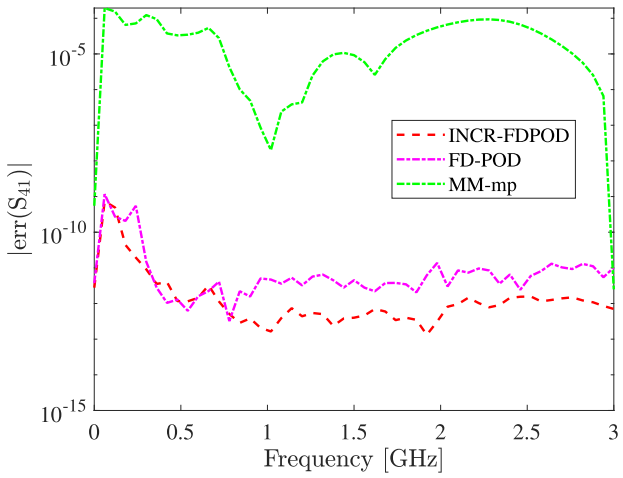

FIGURE 16. Reduced order models error comparison for S_{41} for the two microstrip interconnection example.

B. TWO COPLANAR MICROSTRIPS

In this example, the original PEEC model has an order $n = 20080$ with $n_I = 4$ inputs and $n_O = 4$ outputs. There

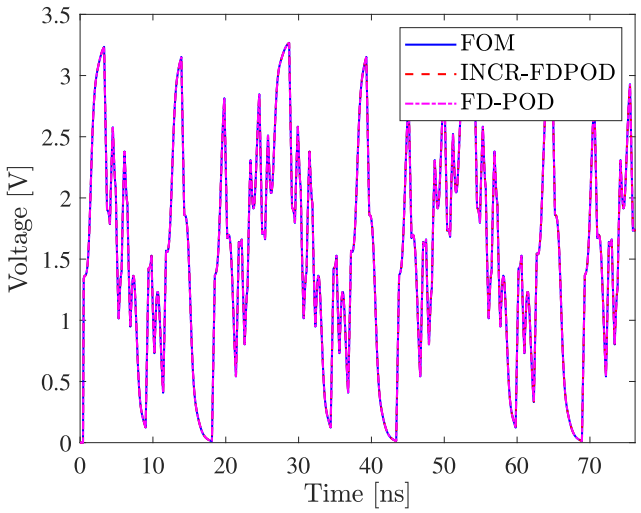

FIGURE 17. Comparison of the input port voltage of the driven line for the two microstrip interconnection example.

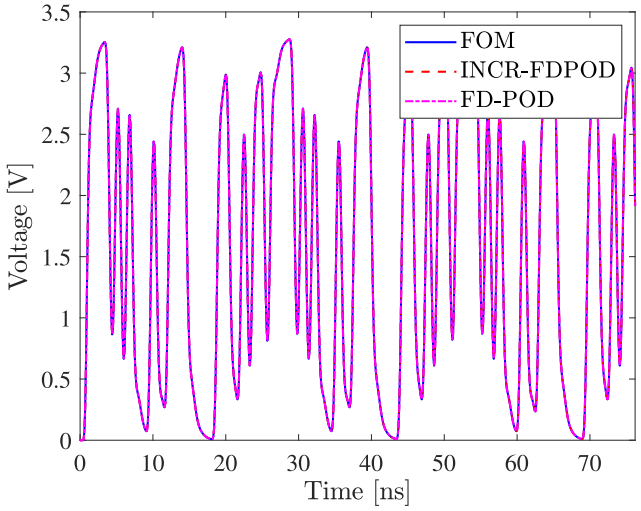

FIGURE 18. Comparison of the output port voltage of the driven line for the two microstrip interconnection example.

are $n_{\tau_L} = 17$ and $n_{\tau_P} = 17$ delays. The geometry of the system is shown in Fig. 8 Using Algorithm 1, we get a POD-based reduced order model of size $r_u = 120$. We use 12 snapshots uniformly distributed in the frequency range [1 MHz, 3 GHz]. The **K** matrix for the INCR-FDPOD method was computed using the INCR-SVD technique, while the FD-POD method utilized the standard one-shot SVD method for this computation. We choose three expansion points for $MM-mp$ [10 Hz, 1 GHz, 3 GHz]. As in the previous example, the CPU time comparison related to the construction of the different reduced order models and the size of each reduced model are shown in Table 4.

Also, we analyze the CPU time needed to evaluate the scattering parameters for a frequency sample by the different models and we illustrate it in Table 5.

To check the precision of the reduced-order models, we examine the responses of the scattering parameters. The

TABLE 4. Construction time and size of the reduced order models for the two microstrip interconnection example.

Model	Size	Construction Time (s)
FOM	20080	-
INCR-FDPOD	120	1720
FD-POD	120	1632
MM-mp	120	19090

TABLE 5. CPU time comparison for a single frequency sample evaluation of the scattering parameters for the two microstrip interconnection example.

Model	Evaluation Time (s)
FOM	104
INCR-FDPOD	$4.497 \cdot 10^{-3}$
FD-POD	$5.764 \cdot 10^{-3}$
MM-mp	$4.457 \cdot 10^{-3}$

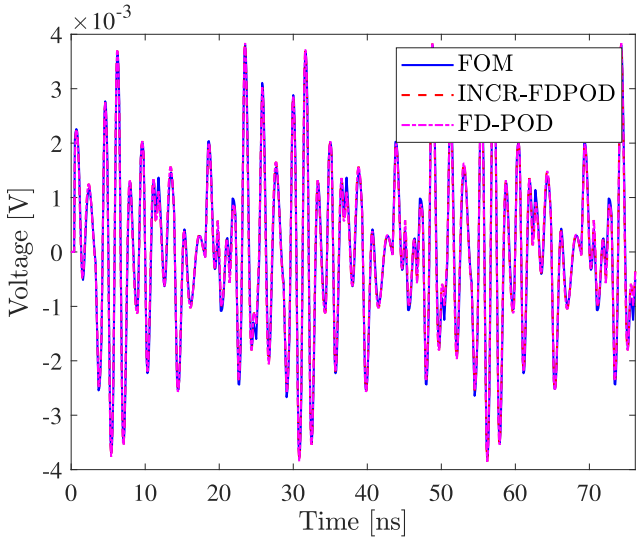

FIGURE 19. Comparison of the input port voltage of the victim line for the two microstrip interconnection example.

magnitude of the scattering parameters S_{11} and S_{21} of the reduced-order models is depicted in Figure 9, and this data is compared to the corresponding parameters of the original PEEC model.

Next, we analyze the magnitude of scattering parameters S_{31} and S_{41} of the original PEEC model and reduced order models which are shown in Figs. 11-12, respectively.

To check the accuracy of both reduced order models, the error analysis for these scattering parameters is plotted in Figs- 13-16.

INCR-FDPOD and FD-POD outperform MM-mp in terms of accuracy for the same reduced order. Subsequently, we examine the results in the time domain by exciting the first input with a PRBS voltage source. The voltage on the first port is depicted in Fig. 17. The output port voltage of the driven line is shown in Fig. 18. The input and output port voltages of the victim line are shown in Figs. 19-20. The results indicate that INCR-FDPOD and FD-POD exhibit better performance in terms of accuracy. While the time-domain simulations of the FOM require 4092 s, both INCR-FDPOD and FD-POD complete the simulation in only 0.9 s.

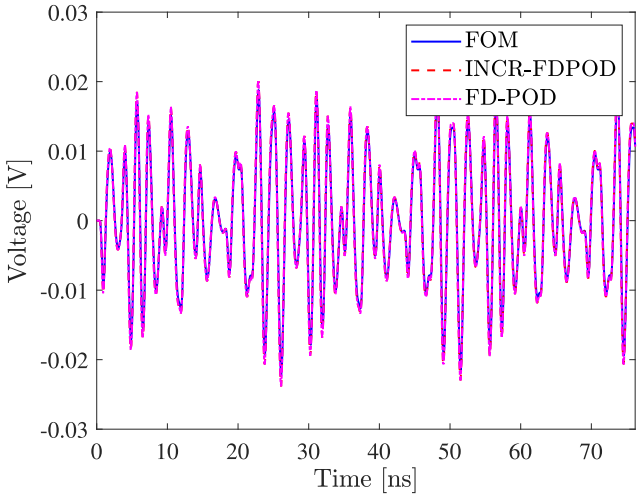

FIGURE 20. Comparison of the output port voltage of the victim line for the two microstrip interconnection example.

Furthermore, the MM-mp results in the time domain are unstable.

VI. CONCLUSION

In this paper, two POD MOR techniques for delayed PEEC models using one-shot and incremental SVD steps have been proposed. A comparison with a moment-matching MOR technique has been also performed. The proposed MOR techniques generate reduced order models with higher accuracy than in the case of moment matching MOR for the same reduced order and they are more efficient in the generation of the reduced order models. Frequency-domain and time-domain results have been shown for multiple numerical examples.

REFERENCES

[1] R. F. Harrington, *Field Computation by Moment Methods*. Piscataway, NJ, USA: Wiley, 1968.
[2] A. E. Ruehli, "Equivalent circuit models for three-dimensional multiconductor systems," *IEEE Trans. Microw. Theory Techn.*, vol. MTT-22, no. 3, pp. 216–221, Mar. 1974.
[3] C. A. Balanis, *Advanced Engineering Electromagnetics*, 2nd ed. Hoboken, NJ, USA: Wiley, 2012.
[4] A. E. Ruehli, G. Antonini, and L. Jiang, *Circuit Oriented Electromagnetic Modeling Using the PEEC Techniques*. Hoboken, NJ, USA: Wiley, 2017.
[5] W. H. Schilders, H. A. van der Vorst, and J. Rommes, Eds., *Model Order Reduction: Theory, Research Aspects and Applications* (The European Consortium for Mathematics in Industry), Berlin, Germany: Springer, Aug. 2008.
[6] D. Romano and G. Antonini, "Partitioned model order reduction of partial element equivalent circuit models," *IEEE Trans. Compon., Packag., Manuf. Technol.*, vol. 4, no. 9, pp. 1503–1514, Sep. 2014.
[7] M. A. Farhan, N. M. Nakhla, M. S. Nakhla, and R. Achar, "Fast transient analysis of tightly coupled interconnects via overlapping partitioning and model-order reduction," *IEEE Trans. Compon., Packag., Manuf. Technol.*, vol. 4, no. 10, pp. 1648–1656, Oct. 2014.
[8] T.-S. Nguyen, T. L. Duc, T.-S. Tran, J.-M. Guichon, O. Chadebec, and G. Meunier, "Adaptive multipoint model order reduction scheme for large-scale inductive PEEC circuits," *IEEE Trans. Electromagn. Compat.*, vol. 59, no. 4, pp. 1143–1151, Aug. 2017.
[9] Y. Dou and K.-L. Wu, "A passive PEEC-based micromodeling circuit for high-speed interconnection problems," *IEEE Trans. Microw. Theory Techn.*, vol. 66, no. 3, pp. 1201–1214, Mar. 2018.

[10] W. Tseng, C. Chen, E. Gad, M. Nakhla, and R. Achar, "Passive order reduction for RLC circuits with delay elements," *IEEE Trans. Adv. Packag.*, vol. 30, no. 4, pp. 830–840, Nov. 2007.
[11] F. Ferranti, M. S. Nakhla, G. Antonini, T. Dhaene, L. Knockaert, and A. E. Ruehli, "Multipoint full-wave model order reduction for delayed PEEC models with large delays," *IEEE Trans. Electromagn. Compat.*, vol. 53, no. 4, pp. 959–967, Nov. 2011.
[12] E. Rasekh and A. Dounavis, "Multiorder Arnoldi approach for model order reduction of PEEC models with retardation," *IEEE Trans. Compon., Packag., Manuf. Technol.*, vol. 2, no. 10, pp. 1629–1636, Oct. 2012.
[13] S. Naderi Lordejani, B. Besselink, A. Chaillet, and N. van de Wouw, "Model order reduction for linear time delay systems: A delay-dependent approach based on energy functionals," *Automatica*, vol. 112, Feb. 2020, Art. no. 108701.
[14] S. N. Lordejani, B. Besselink, A. Chaillet, and N. van de Wouw, *On Extended Model Order Reduction for Linear Time Delay Systems*. Cham, Switzerland: Springer, 2021, pp. 191–215.
[15] K. Afanasiev and M. Hinze, "Adaptive control of a wake flow using proper orthogonal decomposition," in *Shape Optimization and Optimal Design*, vol. 216. New York, NY, USA: Dekker, 2001, pp. 317–332.
[16] H. T. Banks, M. L. Joyner, B. Wincheski, and W. P. Winfree, "Nondestructive evaluation using a reduced-order computational methodology," *Inverse Problems*, vol. 16, no. 4, pp. 929–945, Aug. 2000.
[17] R. Mancini and S. Volkwein, "An inverse scattering problem for the time-dependent Maxwell equations: Nonlinear optimization and model-order reduction," *Numer. Linear Algebra With Appl.*, vol. 20, no. 4, pp. 689–711, Aug. 2013.
[18] Z. Luo and J. Gao, "A POD reduced-order finite difference time-domain extrapolating scheme for the 2D Maxwell equations in a lossy medium," *J. Math. Anal. Appl.*, vol. 444, no. 1, pp. 433–451, Dec. 2016.
[19] T. Kim, "Frequency-domain Karhunen–Loeve method and its application to linear dynamic systems," *AIAA J.*, vol. 36, pp. 2117–2123, Jan. 1998.
[20] G. Dergham, D. Sipp, J.-C. Robinet, and A. Barbagallo, "Model reduction for fluids using frequential snapshots," *Phys. Fluids*, vol. 23, no. 6, Jun. 2011, Art. no. 064101.
[21] W. Wang, G. N. Paraschos, and M. N. Vouvakis, "Fast frequency sweep of FEM models via the balanced truncation proper orthogonal decomposition," *IEEE Trans. Antennas Propag.*, vol. 59, no. 11, pp. 4142–4154, Nov. 2011.
[22] K. T. J. Gladwin and K. J. Vinoy, "An efficient SSFEM-POD scheme for wideband stochastic analysis of permittivity variations," *IEEE Trans. Antennas Propag.*, vol. 71, no. 2, pp. 1654–1661, Feb. 2023.
[23] M. Brand, "Fast low-rank modifications of the thin singular value decomposition," *Linear Algebra Appl.*, vol. 415, no. 1, pp. 20–30, May 2006.
[24] H. Fareed, J. R. Singler, Y. Zhang, and J. Shen, "Incremental proper orthogonal decomposition for PDE simulation data," *Comput. Math. With Appl.*, vol. 75, no. 6, pp. 1942–1960, Mar. 2018.
[25] N. Kühl, H. Fischer, M. Hinze, and T. Rung, "An incremental singular value decomposition approach for large-scale spatially parallel & distributed but temporally serial data—Applied to technical flows," 2023, *arXiv:2302.09149*.
[26] M. A. Khattak, D. Romano, G. Antonini, and F. Ferranti, "Proper orthogonal decomposition-based model order reduction of delayed PEEC models," in *Proc. Int. Conf. Electromagn. Adv. Appl. (ICEAA)*, Venice, Italy, Oct. 2023, pp. 554–558.
[27] R. F. Harrington, *Time-Harmonic Electromagnetic Fields*. Piscataway, NJ, USA: IEEE-Press, 2001.
[28] H. Heeb and A. E. Ruehli, "Three-dimensional interconnect analysis using partial element equivalent circuits," *IEEE Trans. Circuits Syst. I, Fundam. Theory Appl.*, vol. 39, no. 11, pp. 974–982, Nov. 1992.
[29] P. Benner, E. Sachs, and S. Volkwein, "Model order reduction for PDE constrained optimization," *Trends PDE Constrained Optim.*, vol. 165, pp. 303–326, Dec. 2014.
[30] P. Benner, S. Gugercin, and K. Willcox, "A survey of projection-based model reduction methods for parametric dynamical systems," *SIAM Rev.*, vol. 57, no. 4, pp. 483–531, Jan. 2015.
[31] J. Demmel, L. Grigori, M. Hoemmen, and J. Langou, "Communication-optimal parallel and sequential QR and LU factorizations," *SIAM J. Sci. Comput.*, vol. 34, no. 1, pp. A206–A239, Jan. 2012.
[32] *MATLAB Version: 9.10.0 (r2021a)*, Tm Inc., Natick, MA, USA, 2021. [Online]. Available: https://www.mathworks.com

MUHAMMAD A. KHATTAK received the B.S. degree in electrical engineering from the National University of Computer and Emerging Sciences, Islamabad, Pakistan, in 2017, and the M.S. degree in computational science and engineering from the National University of Science and Technology (NUST), Islamabad, in 2022, with a focus on the project funded by the Higher Education Commission, Pakistan. He is currently pursuing the joint Ph.D. degree with the University of L'Aquila, Italy, and Vrije Universiteit Brussel, Belgium.

From 2020 to 2021, he was a Research Assistant with the System Analysis and Control Laboratory, Research Center for Modeling and Simulation, NUST. His research interests include model order reduction, numerical analysis, and complex dynamical systems.

DANIELE ROMANO was born in Campobasso, Italy, in 1984. He received the Laurea degree in computer science and automation engineering and the Ph.D. degree in industrial engineering from the University of L'Aquila, L'Aquila, Italy, in 2012 and 2018, respectively. Since 2012, he has been with the UAq EMC Laboratory, University of L'Aquila, where he is currently a Researcher, focusing on EMC modeling and analysis, algorithm engineering, and speed-up techniques applied to EMC problems.

GIULIO ANTONINI (Senior Member, IEEE) received the Laurea degree (cum laude) in electrical engineering from the University of L'Aquila, L'Aquila, Italy, in 1994, and the Ph.D. degree in electrical engineering from the Sapienza University of Rome, Rome, Italy, in 1998. Since 1998, he has been with the UAq EMC Laboratory, University of L'Aquila, where he is currently a Professor. He has authored more than 300 papers published in international journals and the proceedings of international conferences. He is the coauthored of the book titled *Circuit Oriented Electromagnetic Modeling Using the PEEC Techniques* (Wiley–IEEE Press, 2017). His research interest includes computational electromagnetics.

FRANCESCO FERRANTI (Senior Member, IEEE) received the Ph.D. degree in electrical engineering from Ghent University, Ghent, Belgium, in 2011. He is currently a Professor with the Department of Applied Physics and Photonics, Brussels Photonics, Vrije Universiteit Brussel. He is also an Adjunct Professor with the Indian Institute of Technology (IIT) Madras, Chennai, India, and an Adjunct Professor with Carleton University, Ottawa, ON, Canada. His research interests include data science, machine learning, model order reduction, scientific computing, dynamical systems, electromagnetics, optimization, uncertainty quantification, metasurfaces, nanophotonics, and microwaves. He is a member of the Technical Committee on Design Automation (MTT-2) of the IEEE Microwave Theory and Techniques (MTT) Society. He was a recipient of the Anile-ECMI Prize for Mathematics in Industry 2012 and the Electromagnetic Compatibility Society President's Memorial Award 2012. He is currently an Associate Editor of the IEEE TRANSACTIONS ON MICROWAVE THEORY AND TECHNIQUES. He serves as a regular reviewer for several international journals and conferences.